X-ray Crystal Structure of Human Heme Oxygenase-1 in Complex with 1-(Adamantan-1-yl)-2-(1*H*-imidazol-1-yl)ethanone: A Common Binding Mode for Imidazole-Based Heme Oxygenase-1 Inhibitors[#]

Mona N. Rahman,[†] Jason Z. Vlahakis,[‡] Walter A. Szarek,[‡] Kanji Nakatsu,[§] and Zongchao Jia*[,†]

Departments of Biochemistry, Pharmacology & Toxicology, and Chemistry, Queen's University, Kingston, Ontario K7L 3N6, Canada

Received May 1, 2008

Development of inhibitors specific for heme oxygenases (HOs) should aid our understanding of the HO system and facilitate future therapeutic applications. The crystal structure of human HO-1 complexed with 1-(adamantan-1-yl)-2-(1*H*-imidazol-1-yl)ethanone (**3**) was determined. This inhibitor binds to the HO-1 distal pocket such that the imidazolyl moiety coordinates with heme iron while the adamantyl group is stabilized by a hydrophobic binding pocket. Distal helix flexibility, coupled with shifts in proximal residues and heme, acts to expand the distal pocket, thus accommodating the bulky inhibitor without displacing heme. Inhibitor binding effectively displaces the catalytically critical distal water ligand. Comparison with the binding of 2-[2-(4-chlorophenyl)ethyl]-2-[1*H*-imidazol-1-yl)methyl]-1,3-dioxolane (**2**) revealed a common binding mode, despite differing chemical structures beyond the imidazolyl moiety. The inhibitor binding pocket is flexible, yet contains well-defined subpockets to accommodate appropriate functional groups. On the basis of these structural insights, we rationalize binding features to optimize inhibitor design.

Introduction

Heme oxygenases (HOs[a]) are involved in the regioselective, oxidative cleavage of heme at the α-meso carbon to release equimolar amounts of ferrous iron (Fe^{2+}), carbon monoxide (CO), and biliverdin, the last of which is transformed into bilirubin by biliverdin reductase (Supporting Information Figure S1).[1,2] Indeed, this reaction is the main source of CO in mammals; heme degradation accounts for ∼85% of the CO produced in humans under normal physiological conditions. To date, three HO isozymes have been identified. HO-1, the inducible isoform, is a 32 kDa stress protein found to be induced by a variety of stimuli including heat shock, heavy metals, heme, and reactive oxygen species; HO-1 is predominantly expressed in the spleen.[3] The constitutive isoform, HO-2, is an ∼36.5 kDa protein that is widely distributed and has its highest concentration in the brain and testes. A third isozyme, HO-3, shares ∼90% homology with HO-2 but has been shown to be inactive.[4]

The role of HO in heme catabolism is well understood as is its catalytic mechanism. However, there is increasing evidence regarding the role of CO as a cellular regulator in the brain, blood vessels, and immune systems. Indeed, the CO produced by HO-1 has been shown to have a variety of cellular regulatory actions including anti-inflammatory, antiapoptotic, antiproliferative, and vasodilatory effects.[5−8] CO has been shown to exert many of its effects through the activation of soluble guanylyl cyclase (sGC) and/or mitogen-activated protein kinase (MAPK) signaling pathways.[5,9−12] Furthermore, the HO system has been found to have a protective role in a wide variety of circumstances, such as diabetes, inflammation, heart disease, hypertension, neurological disorders, organ transplantation, and endotoxemia.[13] HO-1 is also a potential target for cancer therapy because the growth of most tumors is dependent on HO-1 activity.[14] Inhibition of HO-1 using a metalloporphyrin inhibitor (pegylated zinc protoporphyrin) has been associated with antitumor activity[15] as well as enhancement of the effects of contemporary anticancer drugs.[16] Thus, there is significant interest in investigating and understanding the CO/HO system.

The development of inhibitors selective for the HO enzymes aims to provide powerful tools for the dissection of the CO/HO system as well as the mechanisms underlying its physiological effects in various pathologies, in addition to future therapeutic applications. Moreover, they may serve as candidates for novel therapies against these diseases. To date, studies have exploited HO inhibitors belonging to the metalloporphyrin class (e.g., tin/zinc/chromium protoporphyrin). However, their close structural similarity to heme results in some nonselectivity because heme plays a key role in a number of biologically relevant enzymes including cytochromes P450, nitric oxide synthase, and soluble guanylyl cyclase. Thus, there have been concerns regarding the validity of the interpretation of the results of these studies.[17−19] The discovery of azalanstat (**1**) (Figure 1), a compound not based on the porphyrin nucleus, as an HO inhibitor led to a program in our laboratory concerned with systematically modifying the structure of **1**, resulting in a series of novel compounds, several of which are HO-1 inhibitors.[20−23] In continuation of our program, a structural study of complexes formed between human HO-1 and some of our selective HO-1 inhibitors was initiated. During the course of these studies, the results of an X-ray crystallographic study of one of our compounds, namely, (2-[2-(4-chlorophenyl)ethyl]-2-[(1*H*-imidazol-1-yl)methyl]-1,3-dioxolane (**2**) were reported (Figure 1).[24] In that study, compound **2** was cocrystallized with heme-conjugated rat HO-1, and it appeared that compound **2** inhibited HO-1 activity by binding to the distal side of the heme iron, thus preventing the oxidation of Fe^{2+} by disrupting a critical hydrogen-bond network and interfering with O_2 binding. [24] In

[#] The hHO-1 complex structure has been deposited into the Protein Data Bank (PDB code 3CZY).

* To whom correspondence should be addressed. Phone: (613) 533-6277. Fax: (613) 533-2497. E-mail: jia@queensu.ca.

[†] Department of Biochemistry.

[‡] Department of Chemistry.

[§] Department of Pharmacology & Toxicology.

[a] Abbreviations: HO, heme oxygenase; sGC, soluble guanylyl cyclase; MAPK, mitogen-activated protein kinase; PMA, phosphomolybdic acid; CHESS, Cornell High Energy Synchrotron Source; MR, molecular replacement; HP, hydrophobic pocket.

10.1021/jm800505m CCC: $40.75
Published on Web 09/18/2008

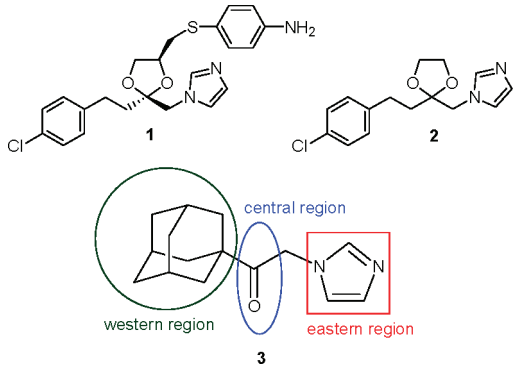

Figure 1. Structures of **1**, **2**, and **3** depicting regions of interest.

Scheme 1[a]

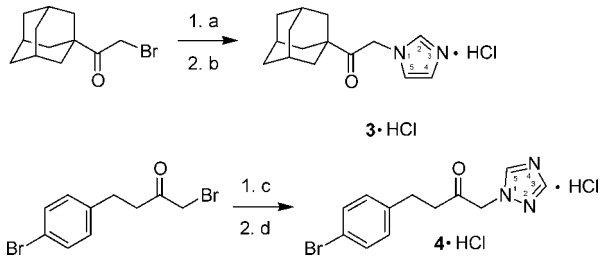

[a] Reagents and conditions: (a) imidazole, *N*,*N*-dimethylformamide, room temp, 7 days; (b) 37% aqueous HCl, EtOH; (c) 1*H*-1,2,4-triazole, *N*,*N*-dimethylformamide, K_2CO_3, room temp, 2 h; (d) 37% aqueous HCl, 2-propanol.

contrast, the metalloporphyrins would compete with heme for binding to the enzyme.

In the present study, we report the crystal structure of human HO-1 in complex with heme and the imidazole-based inhibitor 1-(adamantan-1-yl)-2-(1*H*-imidazol-1-yl)ethanone (**3**) (Figure 1). It is recognized that the structure of **3** is different from that of **2**, yet the ease of formation of the complex of **3** with human HO-1 prompted us to undertake this X-ray crystallographic study. Interestingly, in spite of the structural differences between **3** and the imidazole−dioxolane series of inhibitors, it would appear that there is a common mode of binding, and this information may be useful in the design of more potent inhibitors of HO-1. Our results, in conjunction with those obtained from the previously reported[24] structural study of the complex between rat HO-1 and compound **2**, indeed suggest a common binding mode for our series of structurally related imidazole-based inhibitors[20−23] on the distal side of the heme, in which the flexible distal helix of HO-1 opens up to accommodate the bulky inhibitor. The imidazolyl group serves as an anchor by coordinating with the iron moiety, while the bulky adamantyl group fits into a hydrophobic pocket and is stabilized by hydrophobic interactions. Details of the binding mode were assessed in order to identify factors that could be useful in the future structure-based design of more effective HO-1 inhibitors based on the consideration of different functional groups within the binding pocket.

Results and Discussion

Synthesis and Characterization of Inhibitor 3. In this article, we report the synthesis of compounds **3** and 4-(4-bromophenyl)-1-(1*H*-1,2,4-triazol-1-yl)-2-butanone (**4**). As shown in Scheme 1, compound **3** was synthesized by a nucleophilic displacement reaction on commercially available 1-adamantyl bromomethyl ketone (Sigma-Aldrich) using imidazole in *N*,*N*-dimethylformamide. By use of a similar approach, compound **4** was obtained by a nucleophilic displacement reaction on 1-bromo-4-(4-bromophenyl)-2-butanone[22] using 1*H*-1,2,4-triazole in *N*,*N*-dimethylformamide. The compounds were isolated, characterized, and evaluated as the hydrochloride salts.

Initial screens using a CO formation assay with rat spleen microsomal fractions gave IC_{50} values of 7 ± 1 μM for **3** and 4 ± 2 μM for **2**.[21] The binding of **3** to heme-conjugated recombinant hHO-1 was examined by spectral analysis (Figure 2A). In the absence of inhibitor, the heme-bound hHO-1 gave a characteristic spectrum with a Soret peak at 404 nm. With increasing amounts of **3** (5−50 μM), the Soret peak shifted to longer wavelengths up to 412 nm, at which point it was presumed to have been saturated with inhibitor as seen with the rat HO-1 complexed with **2**.[24] Furthermore, a more prominent shoulder centered at 355 nm was apparent. Secondary peaks centered at 535 and 560 nm increased with increasing concentrations of inhibitor, while a third minor peak at 630 nm decreased and then disappeared at high inhibitor concentrations. Parallel experiments using inhibitor **2** gave similar results. The shift in the Soret peak was suggestive of a change in the heme environment and, thus, putative binding of the inhibitor. Heme degradation in the presence of increasing amounts of inhibitor **3** was then initiated by the addition of L-ascorbic acid (1 mM) and monitored for 90 min. Under these conditions, the reaction reached completion within 60 min in the absence of inhibitor (data not shown). This rate of reaction was chosen to identify differences in inhibition that might otherwise not be observable to any significant extent at a faster rate. Initial rates were determined for each condition by calculating the rate of change of absorbance over the initial 3 min, according to its respective Soret peak. As seen in Figure 2A, the Soret peak shifts maximally at an inhibitor concentration of 25 μM. At this concentration, the initial rate of reaction (as measured at 412 nm) was diminished to 41 ± 7% of the control rate without any inhibitor (as measured at 404 nm) (Figure 2B). As a comparison, the rate was inhibited to 15 ± 4% of control by **2** at this concentration. The Soret peak shifted to 412 nm at a lower concentration of **2** (10 μM) at which the initial rate of reaction was 39 ± 2% that of the control. Spectral analysis following the heme degradation assay revealed the disappearance of the Soret peak in the absence of inhibitor (Figure 2C). As another means of measurement, the height of the Soret peak following the reaction was compared to that in a control experiment in which ascorbic acid was absent. The absorbance of the Soret peak in the absence of inhibitor fell to 24 ± 1%, whereas the height only diminished to 44 ± 5% and 54 ± 5% in the presence of 25 and 50 μM of inhibitor **3**, respectively, further indicating inhibition of heme degradation. In the presence of inhibitor **2** at these concentrations, the absorbance only fell to 65 ± 4% and 80 ± 5%, respectively.

Crystallization and Structure Determination of hHO-1 in Complex with Inhibitor 3. In order to confirm binding of inhibitor **3** prior to attempting cocrystallization trials, spectral analyses were undertaken on both the native protein and that incubated with **3** at a molar ratio of 1:3. After a 15 min incubation of the native protein with inhibitor, the expected shift in the Soret peak from 404 to 412 nm was observed, thus verifying binding. This mixture was subsequently utilized for crystallization trials based on previously known conditions for the native protein.

Cocrystals of hHO-1 bound to **3** were reminiscent of native hHO-1 crystals, growing as clusters of thin plates, a feature that

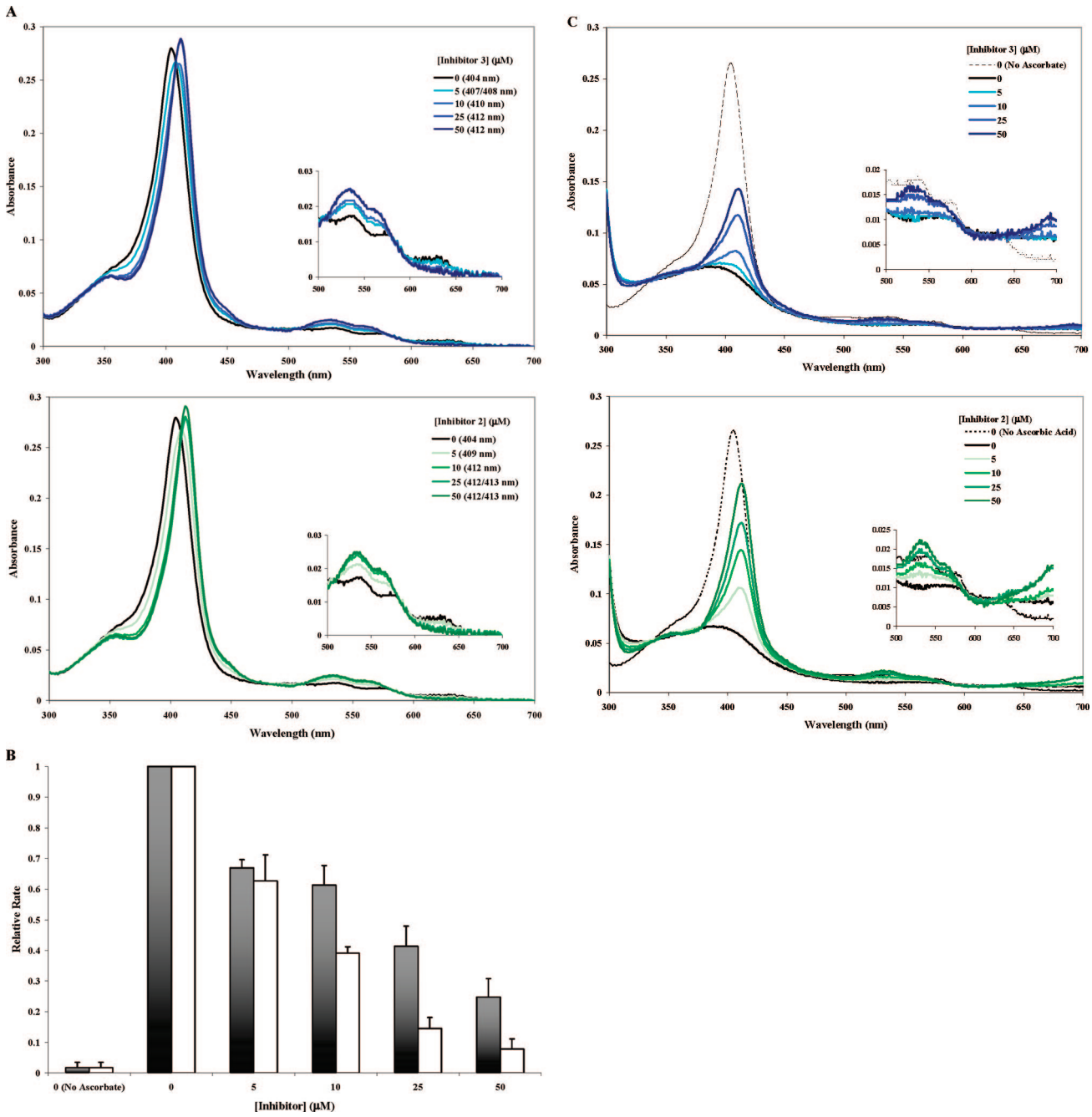

Figure 2. Spectral analysis of **3** binding to hHO-1. (A) Heme-conjugated hHO-1 (10 μM) in 20 mM potassium phosphate (pH 7.4) was incubated with increasing concentrations of **3** (blue) or **2** (green) for 5 min at room temperature. Absorbances were measured over a range of 300−700 nm at intervals of 1 nm, and values were corrected for buffer (20 mM potassium phosphate, pH 7.4). The assays were performed in triplicate and the values averaged. The wavelength corresponding to the Soret peak for each spectrum is indicated. The Soret peak gradually shifted from 404 to 412 nm with increasing concentrations of **3** or **2**, with a more prominent shoulder centered at 355 nm. Secondary peaks centered at 535 and 560 nm were observed to be increased with increasing concentrations of inhibitor, while a third minor peak at 630 nm was observed to decrease until it was no longer detectable at high inhibitor concentrations. (B) Heme degradation rates in the presence of inhibitor **3**. Heme degradation was subsequently initiated by the addition of 1 mM L-ascorbic acid and allowed to proceed for 90 min at room temperature. Absorbances were measured at 404, 408, 410, and 412 nm at 90 s intervals. Initial rates were determined for each condition by calculating the rate of change of absorbance over the initial 3 min, at the wavelength corresponding to its respective Soret peak. For each replicate, values were normalized to the respective control condition and subsequently averaged. Parallel reactions were also performed for heme-conjugated hHO-1 in the absence of both inhibitor and electron donor (L-ascorbic acid) as a negative control (i.e., no oxidative degradation). Shaded bars depict rates in the presence of **3**; open bars depict rates in the presence of **2**. (C) Spectral analysis following heme degradation. Absorbances were measured and analyzed as described in (A). Heme degradation was observed as the disappearance of the Soret peak. Increasing concentrations of inhibitor resulted in increasing attenuation of the loss of the Soret peak as well as of the secondary peaks at 535 and 560 nm but the appearance of a peak at 699 nm.

necessitated careful and challenging separation in order to obtain single crystals. Diffraction data were obtained to a resolution of 1.54 Å for the cocrystal which belongs to the $P2_1$ space group. Because of the new crystal form, molecular replacement was carried out using the native heme-conjugated hHO-1 (PDB code 1N3U) from which heme had been omitted. Two unambiguous solutions were obtained corresponding to the two molecules in the asymmetric unit. The structure of the heme-conjugated hHO-1 bound to **3** was refined to an *R* factor of 0.19 and a free *R* factor of 0.23. The Ramachandran plot showed that 100% of

Table 1. Diffraction and Refinement Statistics[a]

space group	$P2_1$
a (Å)	52.00
b (Å)	52.45
c (Å)	74.49
β (deg)	89.99
molecules in the asymmetric unit	2
solvent content (%)	34
mosaicity (deg)	0.623
resolution range (Å)	50−1.54
total reflections	374747
unique reflections	57555
completeness (%)	97.1 (82.8)
I/σ	36.5 (4.4)
R_{merge}[b]	0.086 (0.356)
average redundancy	6.5 (3.7)
Refinement Statistics	
σ cutoff for refinement	none
R_{crys}[c]	0.194
R_{free}[c]	0.226
number of reflections used	54625
number of reflections in test set	2899
number of non-hydrogen atoms used in refinement	4115
rmsd bond lengths (Å)	0.010
rmsd bond angles (deg)	1.217
number of water molecules	536
ligand occupancy	1.00
Ramachandran Plot	
most favored (%)	95.1
additional allowed (%)	4.9
generously allowed (%)	0.0
disallowed regions (%)	0.0

[a] Values in parentheses are for the outermost shell (1.60−1.54 Å). [b] $R_{merge} = \sum|I_{obs} - \langle I\rangle|/\sum I_{obs}$, where I_{obs} is the intensity measurement and $\langle I\rangle$ is the mean intensity for multiply recorded reflections. [c] R_{cryst} and $R_{free} = (\sum|F_{obs} - F_{calc}|)/(\sum|F_{obs}|)$ for reflections in the working and test sets, respectively.

the residues were in the allowed region. The final statistics are given in Table 1, and the structure has been deposited in the Protein Data Bank (3CZY).

Overall Structure of hHO-1 Bound to 3. The two molecules in the asymmetric unit (A and B) were found to be virtually identical with a Cα rmsd of 0.06 Å (upon alignment of all the atoms). The maximum displacement found is in the flexible, distal helix: Gly144 with 0.39 Å and Gly143 with 0.11 Å. There were also slight differences in the number and placement of water molecules near the active site. Given the closeness in structure of the two molecules in the asymmetric unit, further discussion will focus on the A chain unless otherwise stated.

The overall structure of the hHO-1 complex with **3** was very similar to that of the native heme-conjugated hHO-1,[25] being mostly α-helical with the heme sandwiched between the proximal and distal helices (parts A and B of Figure 3, Supporting Information Figure S2). Inhibitor **3** was bound to the distal side of the heme, as clearly demarcated by the electron density map, with the imidazole ring coordinating the heme iron, i.e., serving as an anchor, at a distance of 2.06 Å (Figure 3A). Alignment of the structure with that of the complex of **2** with the rat HO-1 shows that they are also very close with an rmsd of 0.76 Å (Figure 3C). As seen by the electrostatic surface representation of the molecule, the adamantyl moiety is bound within a hydrophobic pocket that extends back toward the distal side of the heme binding pocket (Figure 4A). Residues lining the distal pocket, which may contribute to hydrophobic interactions, include Phe37, Phe167, Leu54, Met34, and Leu147. A detailed table of residues within van der Waals distance of the inhibitor, which may contribute to its binding, is listed in Supporting Information Table S1. Compared to the native

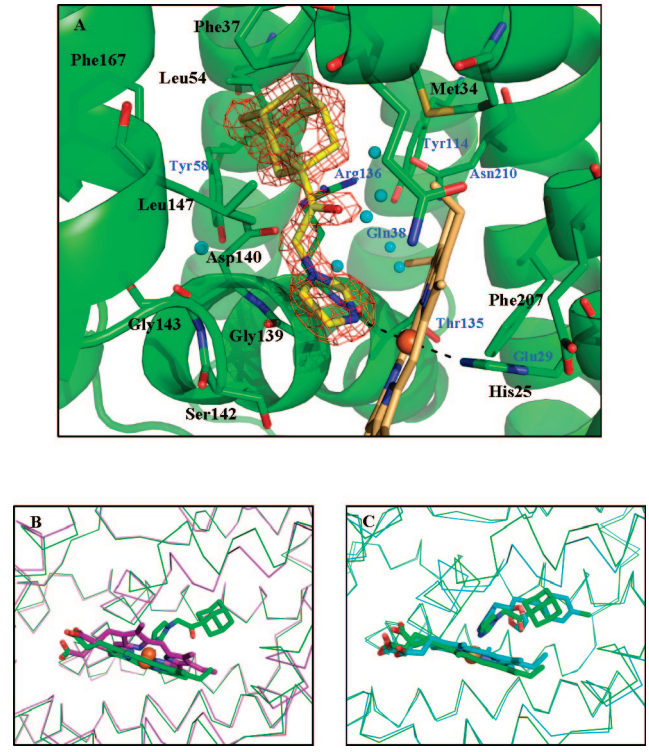

Figure 3. (A) Ribbon diagram of the inhibitor binding site of heme-conjugated hHO-1 in complex with **3** at 1.54 Å resolution. Heme (light orange) and **3** (yellow) are depicted as stick models. An omit map contoured at 3.5σ is superimposed. Dashed lines indicate coordination of imidazole nitrogens of **3** and His25 with the heme Fe. Residues involved in inhibitor binding are indicated (black) as are secondary residues (blue) involved in the Asp140-hydrogen bond network (Tyr58, Tyr114, Arg136, Asn210),[25] and those adjacent to the coordinating His25 residue (Glu29, Gln38, Phe207) which were found to shift in order to accommodate both heme and the inhibitor. The Thr135 residue found to be involved in a hydrogen-bond network with a water molecule and the dioxolane group of **2** in its cocrystal structure with rat HO-1 (PDB code 2DY5)[24] is also indicated. Only water molecules in the distal pocket have been included for simplicity. Backbone monomer traces illustrate the structural alignment of **3** bound to hHO-1 (green) with (B) native hHO-1 holoenzyme (PDB code 1N45, purple) and with (C) **2** bound to rat HO-1 (PDB code 2DY5, cyan). Alignment was performed by (B) fitting all atoms or by (C) secondary structure matching (SSM).

structure and that of the rat HO-1 bound to **2** (parts B and C of Figure 4, respectively), the distal pocket into which **3** binds appears more open than that of either the native or the rat HO-1 bound to **2**. The carbonyl group of Gly139 is close enough to form hydrogen bonds with the coordinating nitrogen of the imidazole group (2.68 Å) as well as weakly interacting with the other nitrogen (3.68 Å), if they were protonated. However, given that the neighboring His25 is a neutral imidazole,[26] it is likely that this is also the case for the imidazole ring of the inhibitor in this environment, so there would be no hydrogen bonds possible. Moreover, there appears to be a secondary hydrophobic pocket adjacent to that binding the adamantyl group which is not as prominent in either the structure of rat HO-1 bound to **2**[24] or the native structure.[25,27]

Changes in the Distal Helix. Comparison of the inhibitor-bound structure to the high resolution (1.5 Å) structure of the presumably more active, "closed" conformation of hHO-1[25] revealed very little change in overall structure with a Cα rmsd of 0.74 Å. The maximum displacement of 3.92 Å (Gly144) corresponds to changes in the distal helix within the heme binding pocket (Figure 3B). Relative to the native structure, in

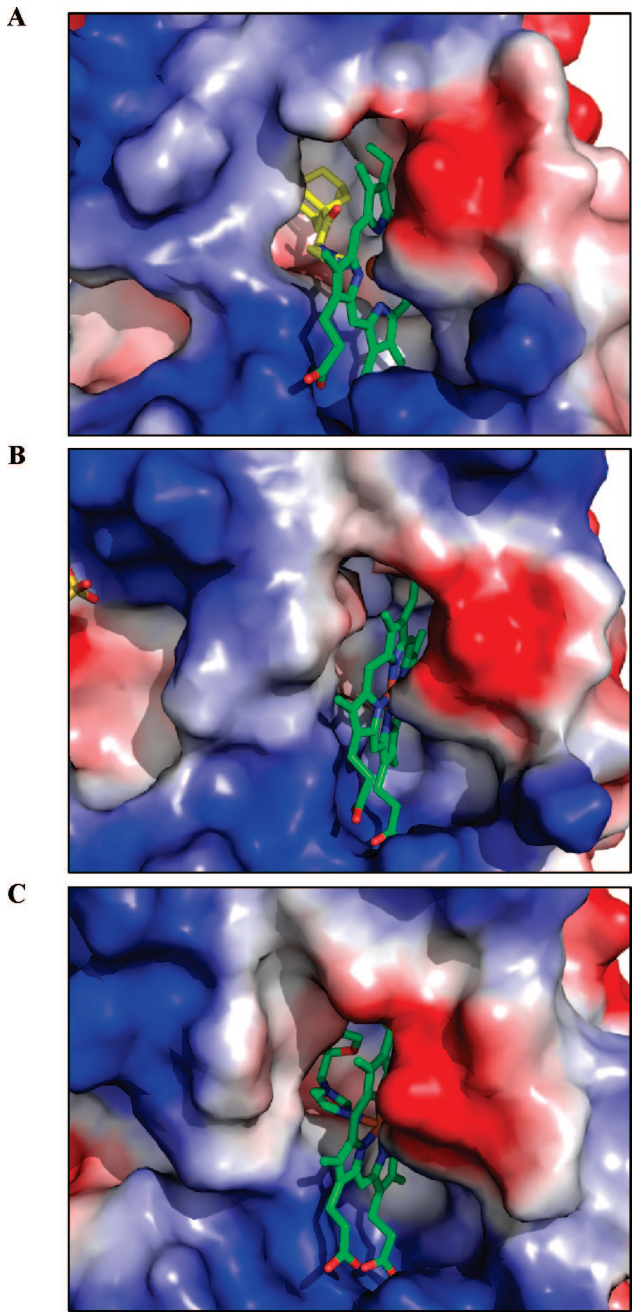

Figure 4. Electrostatic surface potentials of (A) the complex of inhibitor **3** with hHO-1 revealing a hydrophobic pocket into which the adamantyl moiety fits. Comparison of the electrostatic surface potentials of (B) the native human HO-1 holo-enzyme (PDB code 1N45) and (**C**) the complex of **2** with rat HO-1 (PDB code 2DY5) reveals a larger distal pocket in the enzyme bound to **3**. Blue and red colors indicate positive and negative electrostatic potentials, respectively, as calculated using PyMOL. The adamantyl moiety of **3** binds to the hydrophobic pocket in a manner similar to that of the chlorophenyl moiety of **2**. A secondary hydrophobic pocket is also more prominent in hHO-1 bound to **3**.

the presence of **3**, the distal helix is shifted outward from Ser142 to Ile150 to open up the hydrophobic distal pocket. While the shift maintains hydrogen bonding of the alcohol moiety of Ser142 with the ammonium moiety of Lys179 (2.72 Å in the native to 2.79 Å) in the ligated complex, it appears to shift closer to the inhibitor by 1.97 Å. As a result, hydrogen-bonds between the Ser142 alcohol and the heme propionate moiety (3.05 Å) and a solvent water molecule (3.14 Å) are lost, while a new hydrogen bond would be formed with the carbonyl group of Leu138 (2.67 Å). Furthermore, there is a resultant break in the distal helix from Ser142 to Gly144 implying a greater flexibility in this region. A comprehensive analysis of the temperature factors in this region revealed higher than average values for both the native and inhibitor **3**-complexed structures of hHO-1, as well as for rat HO-1 in complex with **2**. However, a difference plot in which the normalized values of the closed, i.e., putatively more active, conformation of the native structure (PDB code 1N45, chain A) were subtracted, revealed no significant increase in the thermal factor values in the distal helix (data not shown). Thus, we conclude that the distortion of the helix in order to accommodate the bulky inhibitor could be accomplished by the inherent helical flexibility, without any further increase in flexibility. It should be noted that in the structure of the native, heme-conjugated HO-1, Ser142 is involved in stabilizing distal helix distortion (i.e., a kink) via hydrogen-bonds with the peptide backbones of Gly143 and Leu141, a distortion that is maintained in the apo-form of the enzyme.[25] Close comparison of hydrogen-bonding patterns with the native structure in this region reveals the loss of backbone hydrogen-bonds involving Ser142, Gly143, Gly144, the amide groups of Leu147 and Lys148, as well as the carbonyl groups of Leu141 and Asp140. Moreover, potential hydrogen-bonds form with water molecules involving the carbonyl groups of Leu141 (2.69 Å) and Asp140 (2.70 Å and 2.71 Å), as well as the amide group of Gly143 (3.12 Å). This last water molecule, which interacts with both Gly143 and Asp140, is situated 4.08 Å from the active nitrogen on the imidazolyl group. In the B molecule, this water may be close enough to form a weak hydrogen-bond (3.86 Å) that may contribute to the stabilization of the imidazolyl group. Interestingly, the structure of rat HO-1 bound to **2**[24] also resulted in the loss of hydrogen-bonds involving Gly139, Asp140, Leu141, Ser142, Gly143, Gly144, Gln145, Leu147, Lys148, and Lys149, yet did not result in breakage of this distal helix, implying that the breakage was caused by the need to accommodate the bulkier adamantyl group of **3**. Thus, there is an inherent flexibility in the distal helix, as already seen with the open and closed forms of the holo- and apo-enzymes,[25,27] that appears to be the basis by which **2** and **3** are able to bind, noncompetitively, to the heme-binding pocket.

Changes within the Distal Pocket. Within the hydrophobic pocket that contains the western region (Figure 1) of **3**, the side chain of Leu147 is shifted by 2.58 Å, relative to the native structure, while the phenyl moiety of Phe37 tilts toward the adamantyl group by 1.3−1.4 Å (Figure 3A). Moreover, both the heme moiety and the coordinating His25 residue are pushed back to further open the distal pocket, with the His25 shifted by 0.91 Å while the Fe moiety is shifted by 0.85 Å. As a result, the distance between the coordinating nitrogen of His25 and Fe is increased to 2.04 Å from 1.99 Å. Similarly, the His25−Fe distance in the B molecule of the inhibitor complex is increased to 2.01 Å from 1.90 Å. Adjacent to the coordinating His25, the phenyl group of Phe207 is also shifted back by 0.4−0.75 Å, while the side chains of Glu29 and Gln38 residues in the proximal side of the heme-binding pocket are shifted back by 1.35 and 2.61 Å, respectively, maintaining the hydrogen-bond between Glu29 and His25 at a distance of 2.83 Å but lengthening the potential hydrogen-bond distance between it and the His25 carbonyl from 2.68 to 2.97 Å. The shift in Gln38 results in it not being able to directly form a hydrogen-bond with Glu29, similar to what is seen in the apo-structure of HO-1 as well as the open form of the holo-enzyme.[25]

Changes in Heme Structure. The heme in the native structure of hHO-1 is puckered, while that in the inhibitor

Table 2. Inhibitory Potency of Imidazole−Dioxolanes, Imidazole−Ketones, and Imidazole−Alcohols

substituent in the western region	electronegativity[b] of halogen atom	IC_{50} (μM)[a] dioxolane	ketone	hydroxyl
p-fluorophenyl	4.0	3.8 ± 1.1[c]	2.7 ± 0.9[c]	1.4 ± 1.1[c]
p-chlorophenyl	3.0	4.3 ± 2.1[d] (**2**)	4.7 ± 0.5[c]	0.5 ± 0.1 μM[c]
p-bromophenyl	2.8	1.9 ± 0.2[c]	1.7 ± 0.7[c] (**5**)	0.14 ± 0.06[c]
p-iodophenyl	2.5	3.7 ± 0.9[c]	0.11 ± 0.06[c]	0.06 ± 0.03[c]
phenyl		0.7 ± 0.4[c]	4.0 ± 1.8[c]	6.2 ± 0.8[c]
adamantyl			3 ± 1 μM (**3**)	

[a] IC_{50} values calculated from CO activity assays using spleen (HO-1) microsomal preparations derived from rats. [b] Electronegativity values as derived by Linus Pauling.[30] [c] Values obtained from Roman *et al.*[22] [d] Value obtained from Vlahakis *et al.*[21]

complex is more planar. As a result there is an "uneven" shift of the α-, β-, δ-, and γ-meso-carbons by 0.82, 2.22, 0.67, and 0.45 Å, respectively. Interestingly, the structure of a D140A mutant of human HO-1 was also found to have a "flatter" heme than the wild-type structure.[28] Heme ruffling has been proposed to increase spin density on the meso carbon atoms to promote electrophilic attack by the ferric hydroperoxo intermediate.[29] Thus, similar to the D140A mutant of HO-1, the binding of inhibitor may alter the ability of HO-1 to adopt the proper heme geometry and electronic state for the rapid electrophilic addition of the peroxide OH group to the α-meso carbon.[28] Of note, in the refinement of the rat HO-1 structure with inhibitor **2**, the structure of the tetrapyrrole moiety of heme was restrained in a planar conformation.[24] It would be interesting to determine whether this change in heme geometry is also a consequence of binding to **2** by refinement without these additional restraints.

Central Region of the Inhibitor. The critical Asp140 residue involved in the hydrogen-bonding network that anchors the heme distal water ligand deemed essential for catalysis is not perturbed by the binding of **3**; each of the oxygen atoms of the carboxylic acid moiety was shifted by only ∼0.2 Å.[25] In the native enzyme, when heme binds, the active site closes and critical water residues are trapped to form this well-ordered solvent structure. The hydrogen-bond network also involves Asn210 and Arg136 to stabilize the critical water residue, with a second tier including Tyr58 and Tyr114.[27] The carbonyl group of Gly139 was also observed to hydrogen-bond with the distal water ligand. Binding of **3** does not perturb the positioning of any of these residues (Figure 3A). However, it does displace the hydrogen-bonded water network such that the distal water ligand is displaced, thus presumably inhibiting heme oxidation, in a manner similar to that proposed for **2**.[24] Close inspection of the electrostatic surface shows that, in contrast to the other structures, a potential channel is apparent alongside Asp140 that is proposed to be involved in proton shuttling via a hydrogen-bonded network of water molecules (Figure 4). The opening of such a channel-like passage may also disrupt the ability of HO-1 to trap water molecules in the heme-binding site. This would be compounded further by the more open conformation of the distal pocket.

In the rat HO-1 structure with **2**, a water molecule hydrogen-bonded to the carbonyl of Thr135 is also weakly bonded to the oxygen atom of the dioxolane group of **2**. However, in the human structure with **3**, the closest water molecule to the ketone functionality is situated 4.02 Å away. It should be noted that the water molecules in this region are probably not static, perhaps because of opening of the cavity to accommodate inhibitor **3**. The fluidity can be seen by comparison of this structure (A molecule) with that of the B molecule which does contain a similar water molecule hydrogen-bonded to the Thr135 carbonyl (2.89 Å), which subsequently forms a hydrogen-bond network with another water molecule (2.67 Å) that may associate weakly with the ketone group of **3** (3.83 Å). This water molecule is also close to the amino group of Arg136 (3.40 Å) and a carboxyl group of Asp140 (3.78 Å). The differences between molecules A and B do diminish the importance of this hydrogen-bond network to the binding of this type of inhibitor to HO-1. Thus, the presence of a ketone or dioxolane group in the central region of the inhibitor may not be a significant mode of binding for this type of inhibitor to HO-1. This latter point was further emphasized upon comparison of the potency of a variety of compounds (i.e., 2-oxy-substituted 1-(1*H*-imidazol-1-yl-4-phenylbutanes), which had been screened using an *in vitro* assay for CO production using microsomal preparations obtained from rat spleen.[22] Manual docking of a few of these compounds in the hHO-1 structure confirmed that their binding would be superimposable to that of **2** and **3** (data not shown). A correlation of the IC_{50} values obtained (Table 2), as well as those similarly obtained for **2** and **3**, revealed that, generally, derivatives containing a hydroxyl in the central region of the molecule were more potent inhibitors than their ketone and dioxolane counterparts.[22] This may be due to the increased hydrogen-bonding potential of the alcohol group to form hydrogen bonds with trapped waters, as well as other residues in the region. For example, its increased rotational flexibility may allow it to be close enough to form a hydrogen-bond with Asp140 and further disrupt the hydrogen-bond network. Given these observations, it may be possible to enhance the potency of the inhibitor by introducing a hydrogen-bond donor functionality that would form a more stable interaction with Asp140, disrupt the hydrogen-bond network, and thus stabilize binding.

Western Region of the Inhibitor. A cursory comparison of various substituents on the phenyl moiety in the western region revealed that, at least for the alcohol derivatives, potency is inversely correlated with electronegativity of the halogen substituent (Table 2).[30] This is to be expected given that this region would bind within the hydrophobic pocket, although the presence of the polar thiol group of Met34 therein may explain why electronegative derivatives in this region are still potent. The observed inhibitory potencies reflected by the electronegativity trend are not as apparent in the dioxolane/ketone series of compounds and may be a result of the increased rigidity of these derivatives. An alternative explanation could be that the larger halogens provide more and better contact. Finally, despite the hydrophobicity of the adamantyl moiety of **3**, its potency is less than that of **2** (Figure 2). Comparison of the two structures reveals that the adamantyl group does not extend as far into the hydrophobic pocket as the chlorophenyl group (Figures 3C and 4). As such, increasing the size of the linker between the ketone and the adamantyl group may increase the potency of this compound.

Secondary Hydrophobic Pocket. The secondary hydrophobic pocket that is apparent upon binding of **3** (Figure 4) may be the region in which the thio-(4-aminophenyl) moiety of

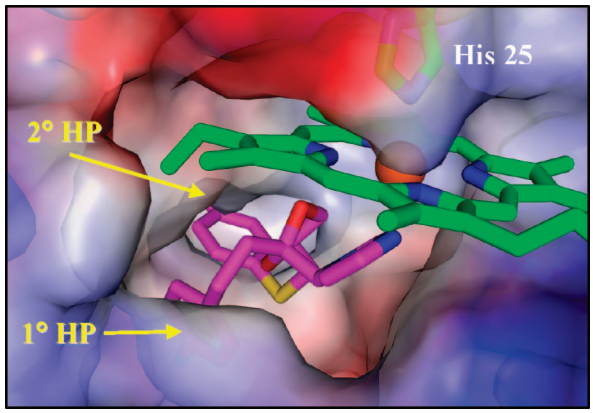

Figure 5. Model of **1** bound to hHO-1. Virtual docking simulation of **1** was performed using AutoDock (version 3.0). The macromolecule used for docking was the A chain of hHO-1 in complex with **3**, in which **3** had been omitted. Electrostatic surface potentials were calculated for hHO-1 bound to **3** as described in Figure 4. Blue and red colors indicate positive and negative electrostatic potentials, respectively. The imidazole moiety coordinates with the heme iron atom, while the chlorophenyl moiety interacts with the primary hydrophobic pocket (1° HP) as with compounds **2** and **3**, while the thio-(4-aminophenyl) group fits easily into the secondary hydrophobic pocket (2° HP) as postulated. The coordinating His25 residue of hHO-1 is shown.

compound **1** analogues interacts.[20,21] The region contains two residues containing polar groups, Ser53 and Met111, that have been replaced by Ala in hHO-2.[31] This may, in part, explain the selectivity of these analogues for HO-1 over HO-2.[20] Thus, while this proximal side of the heme-binding pocket tends to be more rigid than the distal pocket, there is still some flexibility that results in the opening up of the secondary hydrophobic pocket to accommodate such a bulky group in the thio-(4-aminophenyl) region of **1**. Indeed, virtual docking simulation of **1** in the inhibitor binding site of hHO-1 supports this putative interaction (Figure 5).

Implication for Structure-Based Inhibitor Design. As indicated in the Introduction, our initial series of inhibitors are based on **1**, a compound containing an imidazole−dioxolane structural feature. It appears that the results obtained in this study could be useful for the design of such analogues, particularly as regard the choice of substituents of the C4-substituent of the dioxolane ring. The binding of **2** to the heme-binding pocket of HO-1 is merely through hydrophobic interactions and coordination bonding,[24] as in the case of **3**. The flexibility of the heme-binding pocket, mainly through the dynamic nature of the distal helix but also through some shifts of proximal residues and heme itself, allows for the accommodation of these bulky groups by opening up the binding pocket in such a way to bind the inhibitor without displacing heme. As stated before, modifications may be made to take advantage of functional groups within the pocket such as the polar groups in the thio-(4-aminophenyl) region of **1**, disruption of the Asp140-hydrogen bond network, increasing flexibility in the central region, as well as optimizing the length of the central linker to maximize interactions of the western region with the hydrophobic pocket. However, the imidazole moiety of the compounds, by coordination of the heme Fe atom, can be seen as the major force, or the anchor, to this interaction. As such, one means by which potency of binding may be enhanced significantly is by stabilizing this anchor.

The distance between the carbon at position 5 (Scheme 1) of the imidazole ring of **3** and the carbonyl group of Gly139 is 3.21 Å, which is close enough to form a potential hydrogen-bond involving a hydrogen-donating group in this position. Moreover, given the flexibility of the distal helix, it may also be possible to take advantage of a potential hydrogen-bond with the hydroxyl group of Ser142. Of note, the distance between the Cβ of Ser142 and the carbon at position 5 of the imidazole ring is 4.03 Å. Merely rotating the hydroxyl group of Ser142 toward the imidazole ring would allow it to be close enough to form a strong hydrogen-bond. Thus, modification of the imidazolyl moiety to enable this hydrogen-bond formation may be a means by which the potency of the inhibitor can be enhanced. One possibility is the introduction of an amino substituent at position 5 of the imidazole ring, alternatively, replacement of the imidazole ring by a 1,2,4-triazole ring in which the C atom at position 5 of the imidazole is replaced by an N atom. Indeed, we have recently developed a 1,2,4-triazole derivative, namely, 4-(4-bromophenyl)-1-(1*H*-1,2,4-triazol-1-yl)-2-butanone (**4**) (Scheme 1), that takes advantage of the aforementioned hydrogen-bond. As a result, compound **4** exhibited a greater than 4-fold increase in potency compared with its imidazole analogue,[22] namely, 4-(4-bromophenyl)-1-(1*H*-imidazol-1-yl)-2-butanone (**5**) ($IC_{50} = 0.39 \pm 0.07$ μM compared to 1.7 ± 0.7 μM, respectively) (Supporting Information Figure S3).

Conclusion

Inhibitor **3** binds to hHO-1 in a manner similar to that of inhibitor **2** to rat HO-1 despite very different structural features of the inhibitors. Given this, as well as information from modeling other imidazole-containing compounds (data not shown), it appears that all these imidazole-containing compounds bind to HO-1 using a common binding mode. The flexibility of the hHO-1 distal helix allows the heme-binding pocket to expand to accommodate binding of the inhibitor without displacement of the heme moiety, hence in a noncompetitive manner; indeed, a helical break can ensue in the distal helix to accommodate bulkier groups such as the adamantyl moiety. Shifts in the proximal side of the pocket, as well as with heme itself, also contribute to the opening of the distal pocket. As a result, the solvent structure involving Asp140 becomes less ordered. The imidazole group of the inhibitor serves as an anchor with the nitrogen at position 3 coordinating with the heme iron atom, in a manner similar to that of the imidazole group of His25, to result in a hexacoordinate heme Fe. The western region of the inhibitor fits into a hydrophobic pocket on the distal side of the heme-binding pocket, to further stabilize the binding. The central region, while close to the critical Asp140 residue, does not perturb the position of this residue. Rather, inhibition of heme oxidation appears to occur via disruption of the ordered hydrogen-bond network and displacement of the critical water residue required for catalysis by the inhibitor. Further, a secondary hydrophobic pocket may serve as a binding pocket for substituents attached to the C-4 of the dioxolane ring in the imidazole−dioxolane series of compounds. The insights gleaned from the present study may be useful in the design of more potent inhibitors of HO-1.

Experimental Methods

Synthesis. The ^{1}H and ^{13}C NMR spectra were recorded on a Bruker Avance 400 MHz spectrometer in CD_3OD or $CDCl_3$. The signals owing to residual protons in the deuterated solvents were used as internal standards. Chemical shifts (δ) are reported in ppm downfield from tetramethylsilane.[32] High-resolution electrospray mass spectra were recorded on an Applied Biosystems/MDS Sciex QSTAR XL spectrometer with an Agilent HP1100 Cap-LC system. Samples were run in 50% aqueous MeOH at a flow rate of 6 μL/

min. Elemental analyses were performed by MHW Laboratories (Phoenix, AZ). Melting points were determined on a Mel-Temp II melting point apparatus and are uncorrected. Thin-layer chromatography was performed using glass- or aluminum-backed silica gel 60 F_{254} plates (Silicycle). Plates were viewed under UV light or by charring after spraying with phosphomolybdic acid (PMA) in EtOH.

1-(Adamantan-1-yl)-2-(1*H*-imidazol-1-yl)ethanone Hydrochloride (3·HCl). Imidazole (1.56 g, 22.91 mmol, 8 equiv) was added to a solution of 1-(adamantan-1-yl)-2-bromoethanone (735 mg, 2.86 mmol) in *N,N*-dimethylformamide (9 mL) at 0 °C, and the mixture was stirred at 0 °C for 0.5 h, then stirred at room temperature for 7 days (Scheme 1). The mixture was diluted with a saturated aqueous solution of Na_2CO_3, extracted four times with ethyl acetate; the combined organic extracts were washed with brine (2×) and then dried ($MgSO_4$). The solution was dried under high-vacuum to give a pink solid. The solid was ground under H_2O (15 mL) and the mixture stirred at room temperature for 0.5 h. The solid was removed by filtration and washed with H_2O (10 × 10 mL). The pink-white solid was dried under high vacuum to afford the clean free base (545 mg, 2.23 mmol, 78%). To a solution of the free base in warm ethanol (5 mL) was added a solution of 37% aqueous HCl (250 mg, 2.54 mmol, 1.1 equiv) in ethanol (2 mL). The mixture was concentrated and dried under high vacuum. The beige solid was dissolved in a minimum amount of hot ethanol (~4 mL), the solution cooled at −20 °C, and the product allowed to crystallize overnight. The solid was removed by filtration and washed with ethanol (2 × 1 mL). High-vacuum drying afforded **3**·HCl as a beige solid (478 mg, 1.70 mmol, 59%): mp 261−262 °C. ^{1}H NMR (400 MHz, CD_3OD) δ 1.76−1.88 (m, 6H), 1.96−2.00 (m, 6H), 2.06−2.12 (m, 3H), 5.52 (s, 2H), 7.51 (~t, J = 1.6 Hz, 1H), 7.58 (~t, J = 1.6 Hz, 1H), 8.87 (s, 1H). ^{13}C NMR (100 MHz, CD_3OD): δ 29.3, 37.4, 38.9, 46.9, 54.7, 120.4, 124.8, 137.9, 207.3. HRMS (ES) $[M - Cl]^+$ calcd for $C_{15}H_{21}N_2O$: 245.1654. Found: 245.1646.

4-(4-Bromophenyl)-1-(1*H*-1,2,4-triazol-1-yl)-2-butanone Hydrochloride (4·HCl). A mixture of 1-bromo-4-(4-bromophenyl)-2-butanone[22] (306 mg, 1 mmol), 1*H*-1,2,4-triazole (172.5 mg, 2.5 mmol), anhydrous potassium carbonate (345 mg, 2.5 mmol), and anhydrous *N,N*-dimethylformamide (3 mL) was stirred at room temperature for 2 h. The solvent was removed under reduced pressure, and water (30 mL) was added. The mixture was extracted with chloroform (15 mL), and the organic extract was washed sequentially with water (30 mL) and brine (10 mL), dried (sodium sulfate), and concentrated. Purification of the residue by flash column chromatography on silica gel (ethyl acetate) gave the free base **4** as a white solid (279 mg, 0.95 mmol, 95%): mp 118−119 °C. R_f = 0.32 (ethyl acetate). ^{1}H NMR ($CDCl_3$, 400 MHz): δ 2.74 (t, J = 7.2 Hz, 2H), 2.87 (t, J = 7.2 Hz, 2H), 4.93 (s, 2H), 7.02 (d, J = 8.0 Hz, 2H), 7.38 (d, J = 8.0 Hz, 2H), 7.95 (s, 1H), 8.07 (s, 1H). ^{13}C NMR ($CDCl_3$, 100 MHz): δ 28.6, 41.4, 57.8, 120.4, 130.2, 131.8, 139.1, 144.6, 152.3, 201.0. The free base **4** (147 mg, 0.50 mmol) was dissolved in 2-propanol (2.5 mL), treated with 37% HCl (99 mg, 1.00 mmol), and kept for 2 h at room temperature. The solid that precipitated was removed by filtration, washed with diethyl ether, and then recrystallized from 2-propanol−diethyl ether to afford the hydrochloride salt of **4** as a white solid (119 mg, 0.36 mmol, 72%): mp 169−171 °C. ^{1}H NMR (CD_3OD, 400 MHz): δ 2.89−3.01 (m, 4H), 5.46 (s, 2H), 7.17 (d, J = 8.4 Hz, 2H), 7.42 (d, J = 8.4 Hz, 2H), 8.71 (s, 1H), 9.46 (s, 1H). ^{13}C NMR (CD_3OD, 100 MHz): δ 29.3, 41.9, 60.0, 121.0, 131.5, 132.6, 142.2, 146.3, 201.4. HRMS (ESI) calcd for $C_{12}H_{13}BrN_3O$: 294.0242 $[M - Cl]^+$. Found: 294.0243.

Expression and Purification of hHO-1. For crystallization purposes, a truncated, soluble version of hHO-1 was used that contains 233 amino acids (hHO1-t233) and has been employed successfully to solve the high-resolution crystal structure for hHO-1.[25,27,33] Bacterial expression and purification of hHO-1 were based on previously published protocols.[34−36]

Briefly, DH5α cells transformed with the hHO1-t233/pBace expression plasmid[35,37] (a generous gift from Dr. Ortiz de Montellano, University of San Francisco) were grown in 4 L (4 × 1 L) of LB media supplemented with 100 mg/L ampicillin following inoculation from a miniculture. After 18 h of growth, cells were harvested and centrifuged, resulting in green pellets that were stored at −80 °C. Pellets were subsequently thawed on ice, resuspended in lysis buffer (100 mM Tris, pH 8.0; 2 mM EDTA; 2 mM PMSF), and lysed by sonication. Cell debris was separated by centrifugation for 40 min at 15 000 rpm (Beckman JA-20 rotor) at 4 °C. A 35−60% ammonium sulfate pellet was prepared by adding ammonium sulfate to 35% saturation and rocking at 4 °C for 40 min followed by centrifugation for 20 min at 15 000 rpm (JA-20). Ammonium sulfate was added to the supernatant to a final concentration of 60% saturation and rocked for 1 h at 4 °C followed by centrifugation as before. The 35−60% saturated ammonium sulfate pellet was cleared of ammonium sulfate by dialysis against 10 mM potassium phosphate (pH 7.4) prior to further purification. Up to this point, the hHO-1 could be monitored by the presence of green pigment indicative of biliverdin bound to the enzyme, owing to conversion of endogenous heme by the recombinant protein.

The protein was purified further using FPLC over a MonoQ (HR 10/10, Amersham Biosciences) anion-exchange column using a gradient of 0−100 mM KCl in 10 mM potassium phosphate (pH 7.4). Fractions containing the apo hHO-1, as monitored by absorbance (280 nm) and SDS−PAGE analysis, were pooled, and the protein concentration was determined using the Bradford method (Bio-Rad). Apo protein was subsequently combined with a 1.2:1 molar ratio of hemin (Fluka), rocked at 4 °C for 20−30 min, and stored at −20 °C. The excess heme was removed by passage over a PD-10 size-exclusion column (Amersham Biosciences) that had been equilibrated with 20 mM potassium phosphate (pH 7.4). Protein concentration was determined by absorbance (ε_{405} = 140 mM^{-1} cm^{-1}). Purity was assessed by measurement of the R_z ratio (A_{405}/A_{280} > 2.1) and by SDS−P AGE analysis.

CO Activity Assay. HO activity in rat spleen microsomal fractions was determined by the quantitation of CO formed from the degradation of methemalbumin (heme complexed with albumin).[38,39] Incubations for HO activity analysis were done under conditions for which the rate of CO formation (pmol CO min^{-1} mg $protein^{-1}$) was linear with respect to time and microsomal protein concentration. Briefly, reactions mixtures (150 μL) each consisting of 100 mM phosphate buffer (pH 7.4), 50 μM methemalbumin, and 1 mg/mL protein were preincubated with inhibitor (as the HCl salt) at final concentrations ranging from 0.1 to 100 μM for 10 min at 37 °C. Reactions were initiated by adding NADPH at a final concentration of 1 mM, and incubations were performed for an additional 15 min at 37 °C. Blanks for which NADPH was omitted were subtracted to correct for CO that may have formed extraneous to HO activity. Reactions were stopped by instantly freezing the reaction mixture on dry ice, and CO formation was monitored by gas chromatography according to the method described by Vreman and Stevenson.[38]

Spectral Analyses. Inhibitor binding and heme degradation assays were performed by measuring absorbance data using a microplate spectrophotometer (Bio-Tek Instruments). Inhibitor binding was determined by incubation of 10 μM heme-conjugated hHO-1 with increasing concentrations of **3** (0−50 μM) in 20 mM potassium phosphate buffer (pH 7.4) for 5 min at room temperature. Spectra were recorded between 300 and 700 nm at 1 nm intervals. As a reference, assays were also performed in parallel with **2** in place of **3**. After the determination of the Soret peak position, heme degradation was initiated by the addition of L-ascorbic acid to a final concentration of 1 mM and followed by measuring absorbance at the wavelength corresponding to the respective Soret peaks (404, 408, 410, and 412 nm, respectively) at 1.5 min intervals for a period of 90 min. Initial rates of decrease of the Soret band were calculated at the wavelengths of the respective Soret peaks. Spectra were measured from 300 to 700 nm following the reaction period.

Crystallization. Crystallization conditions were based on previously published protocols.[25,27,33] Briefly, sitting-drop vapor diffusion trials were performed at room temperature using a reservoir solution containing 100 mM HEPES (pH 7.5), 2.04−2.24 M ammonium sulfate, and 0.8−1.1% 1,6-hexanediol. The heme−hHO-1

complex (431 μM in 20 mM potassium phosphate) was mixed with **3** at a molar ratio of 1:3 and incubated for 15 min at room temperature. Binding was confirmed using spectral analysis by examining changes in the native Soret peak (described above) prior to setting up crystallization plates. Drops consisted of 2 μL protein−inhibitor solution mixed with 2 μL of reservoir solution.

Data Collection and Structure Determination. X-ray diffraction measurements were performed at the F1 beamline of the Cornell High Energy Synchrotron Source (CHESS). For data collection a cryoprotectant comprising 100 mM HEPES (pH 7.5), 2.32 M ammonium sulfate, 0.9% 1,6-hexanediol, and 20% (v/v) glycerol was used. Crystals were subsequently flash-cooled in a stream of N_2 at 100 K. Data were collected for 360° with an oscillation of 1° and exposure time of 5 s and processed using HKL2000.[40] The structure of the protein−inhibitor complex was solved by molecular replacement (MR) using Phaser. The heme−hHO-1 complex (PDB code 1N3U) in which the heme had been omitted was the initial probe. An initial template of inhibitor **3** was generated using CS Chem3D Ultra (version 6.0, copyright 2000, CambridgeSoft.com) and the Dundee PRODRG2 server.[41] Following initial refinement with Refmac, the structures, first of heme and then of inhibitor **3**, were manually inserted and subsequently refined using iterative cycles of Xfit and Refmac5 in the CCP4 suite.[42] Standard parameters for heme were used as described in its library entry in the program during refinement, with no additional restraints on planarity, bond lengths, and bond angles. Structural alignments were performed using CCP4[42] or DaliLite.[43] Electrostatic surface potentials were calculated using PyMOL.[44] All images were prepared using PyMOL.

Molecular Modeling of 1 in the Inhibitor Binding Site of hHO-1. An initial template of compound **1** was generated as described above for **3**. Virtual docking simulation of **1** was performed using AutoDock (version 3.0).[45] The macromolecule used for docking was the A chain of hHO-1 in complex with **3**, in which **3** had been omitted.

Acknowledgment. This research was supported by CIHR Grant MOP64305 held by Dr. Kanji Nakatsu and Dr. Walter Szarek. Dr. Zongchao Jia holds a Canada Research Chair in Structural Biology. The X-ray data were collected at the Cornell High Energy Synchrotron Source. We thank Dr. Paul Ortiz de Montellano and Dr. John Evans (both from the University of San Francisco) for the generous gift of the hHO1-t233 plasmid and advice regarding its expression. We are grateful to Dr. Qilu Ye and Jimin Zhang for technical expertise in structural determination, Tracy Gifford for her assistance with the biological evaluations, and John G. Riley for the synthesis of compound **4**. We also thank Dr. Gheorghe Roman for helpful discussions.

Supporting Information Available: (1) Oxidative degradation of heme in the carbon monoxide/heme oxygenase (CO/HO) pathway, (2) structure of heme-conjugated hHO-1 in complex with **3** at 1.54 Å resolution, (3) structures of the HO-1 inhibitors, (4) contacts between heme conjugated hHO-1 and **3**, (5) elemental analysis results. This material is available free of charge via the Internet at http://pubs.acs.org.

References

(1) Maines, M. D. The heme oxygenase system: a regulator of second messenger gases. *Annu. Rev. Pharmacol. Toxicol.* **1997**, *37*, 517–554.
(2) Vreman, H. J.; Wong, R. J.; Stevenson, D. K. In *Carbon Monoxide and Cardiovascular Function*; Wang, R., Ed.; CRC Press: Boca Raton, FL, 2002; p 273.
(3) Maines, M. D. Heme oxygenase: function, multiplicity, regulatory mechanisms, and clinical applications. *FASEB J.* **1988**, *2*, 2557–2568.
(4) Hayashi, S.; Omata, Y.; Sakamoto, H.; Higashimoto, Y.; Hara, T.; Sagara, Y.; and Noguchi, M. Characterization of rat heme oxygenase-3 gene. Implication of processed pseudogenes derived from heme oxygenase-2 gene. *Gene* **2004**, *336*, 241–250.
(5) Ryter, S. W.; Alam, J.; Choi, A. M. Heme oxygenase-1/carbon monoxide: from basic science to therapeutic applications. *Physiol. Rev.* **2006**, *86*, 583–650.
(6) Lee, T. S.; Chau, L. Y. Heme oxygenase-1 mediates the anti-inflammatory effect of interleukin-10 in mice. *Nat. Med.* **2002**, *8*, 240–246.
(7) Lee, T. S.; Tsai, H. L.; Chau, L. Y. Induction of heme oxygenase-1 expression in murine macrophages is essential for the anti-inflammatory effect of low dose 15-deoxy-delta 12,14-prostaglandin J2. *J. Biol. Chem.* **2003**, *278*, 19325–19330.
(8) Imuta, N.; Hori, O.; Kitao, Y.; Tabata, Y.; Yoshimoto, T.; Matsuyama, T.; Ogawa, S. Hypoxia-mediated induction of heme oxygenase type I and carbon monoxide release from astrocytes protects nearby cerebral neurons from hypoxia-mediated apoptosis. *Antioxid. Redox. Signaling* **2007**, *9*, 543–552.
(9) Brouard, S.; Otterbein, L. E.; Anrather, J.; Tobiasch, E.; Bach, F. H.; Choi, A. M.; Soares, M. P. Carbon monoxide generated by heme oxygenase 1 suppresses endothelial cell apoptosis. *J. Exp. Med.* **2000**, *192*, 1015–1026.
(10) Brouard, S.; Berberat, P. O.; Tobiasch, E.; Seldon, M. P.; Bach, F. H.; Soares, M. P. Heme oxygenase-1-derived carbon monoxide requires the activation of transcription factor NF-kappa B to protect endothelial cells from tumor necrosis factor-alpha-mediated apoptosis. *J. Biol. Chem.* **2002**, *277*, 17950–17961.
(11) Kim, H. P.; Ryter, S. W.; Choi, A. M. CO as a cellular signaling molecule. *Annu. Rev. Pharmacol. Toxicol.* **2006**, *46*, 411–449.
(12) Liu, X. M.; Chapman, G. B.; Wang, H.; Durante, W. Adenovirus-mediated heme oxygenase-1 gene expression stimulates apoptosis in vascular smooth muscle cells. *Circulation* **2002**, *105*, 79–84.
(13) Abraham, N. G.; Kappas, A. Pharmacological and clinical aspects of heme oxygenase. *Pharmacol. Rev.*, in press.
(14) Fang, J.; Akaike, T.; and Maeda, H. Antiapoptotic role of heme oxygenase (HO) and the potential of HO as a target in anticancer treatment. *Apoptosis* **2004**, *9*, 27–35.
(15) Fang, J.; Sawa, T.; Akaike, T.; Akuta, T.; Sahoo, S. K.; Khaled, G.; Hamada, A.; and Maeda, H. In vivo antitumor activity of pegylated zinc protoporphyrin: targeted inhibition of heme oxygenase in solid tumor. *Cancer Res.* **2003**, *63*, 3567–3574.
(16) Fang, J.; Sawa, T.; Akaike, T.; Greish, K.; Maeda, H. Enhancement of chemotherapeutic response of tumor cells by a heme oxygenase inhibitor, pegylated zinc protoporphyrin. *Int. J. Cancer* **2004**, *109*, 1–8.
(17) Luo, D.; Vincent, S. R. Metalloporphyrins inhibit nitric oxide-dependent cGMP formation in vivo. *Eur. J. Pharmacol.* **1994**, *267*, 263–267.
(18) Meffert, M. K.; Haley, J. E.; Schuman, E. M.; Schulman, H.; and Madison, D. V. Inhibition of hippocampal heme oxygenase, nitric oxide synthase, and long-term potentiation by metalloporphyrins. *Neuron* **1994**, *13*, 1225–1233.
(19) Grundemar, L.; Ny, L. Pitfalls using metalloporphyrins in carbon monoxide research. *Trends Pharmacol. Sci.* **1997**, *18*, 193–195.
(20) Vlahakis, J. Z.; Kinobe, R. T.; Bowers, R. J.; Brien, J. F.; Nakatsu, K.; Szarek, W. A. Synthesis and evaluation of azalanstat analogues as heme oxygenase inhibitors. *Bioorg. Med. Chem. Lett.* **2005**, *15*, 1457–1461.
(21) Vlahakis, J. Z.; Kinobe, R. T.; Bowers, R. J.; Brien, J. F.; Nakatsu, K.; and Szarek, W. A. Imidazole−dioxolane compounds as isozyme-selective heme oxygenase inhibitors. *J. Med. Chem.* **2006**, *49*, 4437–4441.
(22) Roman, G.; Riley, J. G.; Vlahakis, J. Z.; Kinobe, R. T.; Brien, J. F.; Nakatsu, K.; Szarek, W. A. Heme oxygenase inhibition by 2-oxy-substituted 1-(1*H*-imidazol-1-yl)-4-phenylbutanes: effect of halogen substitution in the phenyl ring. *Bioorg. Med. Chem.* **2007**, *15*, 3225–3234.
(23) Kinobe, R. T.; Vlahakis, J. Z.; Vreman, H. J.; Stevenson, D. K.; Brien, J. F.; Szarek, W. A.; Nakatsu, K. Selectivity of imidazole−dioxolane compounds for in vitro inhibition of microsomal haem oxygenase isoforms. *Br. J. Pharmacol.* **2006**, *147*, 307–315.
(24) Sugishima, M.; Higashimoto, Y.; Oishi, T.; Takahashi, H.; Sakamoto, H.; Noguchi, M.; Fukuyama, K. X-ray crystallographic and biochemical characterization of the inhibitory action of an imidazole−dioxolane compound on heme oxygenase. *Biochemistry* **2007**, *46*, 1860–1867.
(25) Lad, L.; Schuller, D. J.; Shimizu, H.; Friedman, J.; Li, H.; Ortiz de Montellano, P. R.; Poulos, T. L. Comparison of the heme-free and bound crystal structures of human heme oxygenase-1. *J. Biol. Chem.* **2003**, *278*, 7834–7843.
(26) Sun, J.; Wilks, A.; Ortiz de Montellano, P. R.; Loehr, T. M. Resonance Raman and EPR spectroscopic studies on heme−heme oxygenase complexes. *Biochemistry* **1993**, *32*, 14151–14157.
(27) Schuller, D. J.; Wilks, A.; Ortiz de Montellano, P. R.; Poulos, T. L. Crystal structure of human heme oxygenase-1. *Nat. Struct. Biol.* **1999**, *6*, 860–867.
(28) Lad, L.; Wang, J.; Li, H.; Friedman, J.; Bhaskar, B.; Ortiz de Montellano, P. R.; Poulos, T. L. Crystal structures of the ferric, ferrous, and ferrous−NO forms of the Asp140Ala mutant of human heme

oxygenase-1: catalytic implications. *J. Mol. Biol.* **2003**, *330*, 527–538.

(29) Rivera, M.; Caignan, G. A.; Astashkin, A. V.; Raitsimring, A. M.; Shokhireva, T. K.; Walker, F. A. Models of the low-spin iron(III) hydroperoxide intermediate of heme oxygenase: magnetic resonance evidence for thermodynamic stabilization of the d(xy) electronic state at ambient temperatures. *J. Am. Chem. Soc.* **2002**, *124*, 6077–6089.

(30) Ebing, D. D. *General Chemistry*; Houghton Mifflin Company: Boston, MA, 1996.

(31) Bianchetti, C. M.; Yi, L.; Ragsdale, S. W.; Phillips, G. N., Jr. Comparison of apo- and heme-bound crystal structures of a truncated human heme oxygenase-2. *J. Biol. Chem.* **2007**, *282*, 37624–37631.

(32) Gottlieb, H. E.; Kotlyar, V.; Nudelman, A. NMR chemical shifts of common laboratory solvents as trace impurities. *J. Org. Chem.* **1997**, *62*, 7512–7515.

(33) Schuller, D. J.; Wilks, A.; Ortiz de Montellano, P. R.; Poulos, T. L. Crystallization of recombinant human heme oxygenase-1. *Protein Sci.* **1998**, *7*, 1836–1838.

(34) Wilks, A.; Ortiz de Montellano, P. R. Rat liver heme oxygenase. High level expression of a truncated soluble form and nature of the meso-hydroxylating species. *J. Biol. Chem.* **1993**, *268*, 22357–22362.

(35) Wilks, A.; Black, S. M.; Miller, W. L.; Ortiz de Montellano, P. R. Expression and characterization of truncated human heme oxygenase (hHO-1) and a fusion protein of hHO-1 with human cytochrome P450 reductase. *Biochemistry* **1995**, *34*, 4421–4427.

(36) Wang, J.; Niemevz, F.; Lad, L.; Huang, L.; Alvarez, D. E.; Buldain, G.; Poulos, T. L.; Ortiz de Montellano, P. R. Human heme oxygenase oxidation of 5- and 15-phenylhemes. *J. Biol. Chem.* **2004**, *279*, 42593–42604.

(37) Wilks, A.; Medzihradszky, K. F.; Ortiz de Montellano, P. R. Heme oxygenase active-site residues identified by heme-protein cross-linking during reduction of CBrCl3. *Biochemistry* **1998**, *37*, 2889–2896.

(38) Vreman, H. J.; Stevenson, D. K. Heme oxygenase activity as measured by carbon monoxide production. *Anal. Biochem.* **1988**, *168*, 31–38.

(39) Cook, M. N.; Nakatsu, K.; Marks, G. S.; McLaughlin, B. E.; Vreman, H. J.; Stevenson, D. K.; Brien, J. F. Heme oxygenase activity in the adult rat aorta and liver as measured by carbon monoxide formation. *Can. J. Physiol. Pharmacol.* **1995**, *73*, 515–518.

(40) Otwinowski, Z.; Minor, W. Processing of X-ray diffraction data collected in oscillation mode. *Macromol. Crystallogr., Part A* **1997**, *276*, 307–326.

(41) Schuttelkopf, A. W.; van Aalten, D. M. PRODRG: a tool for high-throughput crystallography of protein−ligand complexes. *Acta Crystallogr., Sect. D.: Biol. Crystallogr.* **2004**, *60*, 1355–1363.

(42) Collaborative Computational Project, Number 4. The CCP4 suite: programs for protein crystallography. *Acta Crystallogr., Sect. D.: Biol. Crystallogr.* **1994**, *50*, 760−763.

(43) Holm, L.; Park, J. DaliLite workbench for protein structure comparison. *Bioinformatics* **2000**, *16*, 566–567.

(44) DeLano, W. L. *The PyMOL Molecular Graphics System*, version 0.99rc6; DeLano Scientific: Palo Alto, CA, 2002.

(45) Morris, G. M.; Goodsell, D. S.; Halliday, R. S.; Huey, R.; Hart, W. E.; Belew, R. K.; Olson, A. J. Automated docking using a Lamarckian genetic algorithm and an empirical binding free energy function. *J. Comput. Chem.* **1998**, *19*, 1639–1662.

JM800505M